Properties of axisymmetric Bernstein modes in an infinite-length non-neutral plasma

Grant W. Hart and Ross L. Spencer

Properties of axisymmetric Bernstein modes in an infinite-length non-neutral plasma

Grant W. Hart and Ross L. Spencer

Department of Physics and Astronomy, Brigham Young University, Provo, Utah 84602, USA

We have observed axisymmetric Bernstein modes in an infinite-length particle-in-cell code simulation of a non-neutral plasma. The plasmas considered were in global thermal equilibrium and there were at least 50 Larmor radii within the plasma radius. The density of the plasma in the simulation is parameterized by β, the ratio of the central density to the density at the Brillouin limit. These modes have $m = 0$ and $k_z = 0$, where the eigenfunctions vary as $e^{i(m\theta + k_z z)}$. The modes exist both near the Coriolis-shifted (by the plasma rotation) upper-hybrid frequency, $\omega_{uh} = \sqrt{\omega_c^2 - \omega_p^2}$, and near integer multiples (2, 3, etc.) of the Coriolis-shifted cyclotron frequency (called the vortex frequency, $\omega_v = \sqrt{\omega_c^2 - 2\omega_p^2}$). The two modes near ω_{uh} and $2\omega_v$ are the main subject of this paper. The modes observed are clustered about these two frequencies and are separated in frequency at low plasma density roughly by $\delta\omega \approx 10(r_L/r_p)^2 \omega_p^2/\omega_c$. The radial velocity field of the modes has a $J_1(kr)$ dependence in the region of the plasma where the density is nearly constant. For any given density, there are three classes of modes that exist: (1) The fundamental mode is slightly above the upper-hybrid frequency, (2) the upper branch is above the higher of ω_{uh} and $2\omega_v$, and (3) the lower branch is below the lower of ω_{uh} and $2\omega_v$, with similar values of k for both the upper and the lower frequency branches. The modes are fully kinetic and the resulting pressure tensor has significant anisotropy, including off-diagonal terms. A Vlasov analysis of these modes considering only particle resonances up to $2\omega_v$ produces a radial mode differential equation whose solution agrees well with the simulations, except at high density (β greater than about 0.9) where higher-order resonances become important. © 2013 AIP Publishing LLC. [http://dx.doi.org/10.1063/1.4821978]

I. INTRODUCTION

Bernstein waves are electrostatic oscillations perpendicular to the magnetic field near harmonics of the cyclotron frequency.[1] These modes are not correctly described by fluid models of the plasma, but must be described by a fully kinetic theory. The non-zero electric field and equilibrium rotation of the plasma cause these modes to behave differently in a non-neutral plasma than they do in a neutral plasma. The formal kinetic dispersion relation for these waves in an infinite cylindrical non-neutral plasma with uniform density was derived by Davidson,[2] but many details have gone unstudied. Prasad, Morales, and Fried[3] studied these effects in a slab geometry and found that the equilibrium electric field of the plasma shifts the frequency of the single particle gyrofrequency down from the cyclotron frequency. One of the effects of the equilibrium rotation is that the cyclotron frequency is Coriolis shifted in the lab frame of reference. This shifted frequency is called the vortex frequency with magnitude, $|\omega_v| = |\omega_c| - 2|\omega_0|$, where ω_0 is the equilibrium rotation frequency of the plasma.[4,5] Note that throughout this paper $\omega_c = qB/m$ and that this and all other frequencies are signed quantities, e.g., $\omega_c < 0$ for electrons.

In cylindrical geometry, there are families of Bernstein modes that behave as $e^{i(m\theta + k_z z)}$. The modes for $m \geq 1$ for finite temperature have been described and measured by Gould and LaPointe.[6] There was an alternative cold-fluid theory proposed for these same modes by Book.[7] Dubin[8]

described the theory of cold, non-neutral spheroidal plasmas, including high-frequency modes, but that theory does not address the infinitely long plasmas considered here. Recently, Dubin[9] has also examined the theory of both surface cyclotron waves and Bernstein waves in infinitely long plasmas with non-uniform density, but he restricts his attention to $\omega_p^2 \ll \omega_c^2$ and so does not study these modes close to the Brillouin limit as is done in this paper. The ω_{20} mode discussed by Bollinger *et al.*[5] is the spheroidal analog of the fundamental mode discussed in this paper. The breathing mode discussed by Barlow *et al.*[10] appears to be this same mode in a finite-length, low-density system and was used by them and others in the mass spectrometry community to take moderate resolution mass spectra of the confined particles.

This paper is restricted to the $m = 0$ (axisymmetric) case with $k_z = 0$. Such modes would be challenging to see experimentally, because they induce no changes in the wall surface-charge density. By Gauss' law, the perturbed electric field at the wall must be zero. But for finite length plasmas, with the plasma length long compared to the plasma radius, so that an infinitely long theory could give nearly the correct mode frequencies, the property of electrostatic modes that the electrostatic potential at the plasma ends is approximately zero[11] gives the modes a $\cos(k_z z)$ dependence that would produce observable charge on the conducting wall near the center of the plasma. This effect was observed in a

20, 102101-1

recent (r, z) simulation of these modes.[12] The work presented here, however, is restricted to infinitely long plasmas.

This paper proceeds as follows. Section II discusses the simulations used to detect and measure the modes. Section III is a discussion of the kinetic theory of the modes and how to predict their frequencies and radial wavenumbers. Section IV contains the results of the simulations and the comparison of those results to an approximate theory. In most cases they agree reasonably well, but without a detailed analysis of the complex orbits in the plasma edge, high accuracy is not possible. In Sec. V, we discuss the results and draw conclusions.

II. SIMULATION

These modes were first observed in a 2-dimensional cylindrical (r, θ) Particle-in-Cell (PIC) simulation of an infinite-length non-neutral plasma. That code was being used to study possible Fourier-Transform Ion-Cyclotron-Resonance Mass Spectrometry (FTICR-MS) signals in a non-neutral ion plasma.[13] As the modes that were observed were clearly axisymmetric and because the 2D code was slow, a one-dimensional (1D) simulation was written which was much more efficient to run. The results of the 1D code were compared with the results of the 2D code and they agreed within the inherent noise of the simulations. All of the results given below are from the 1D code.

A. 1D particle-in-cell code

Because these modes have only r-variation in cylindrical geometry, they can be studied by means of a one-dimensional code. In many ways, this code is a standard PIC code, but it has two main modifications. These are (1) that it uses $x = r^2$ as the radial variable and (2) that it solves for E_r by using Gauss' law, since the plasma is axisymmetric. The reason for using $x = r^2$ as the independent variable has to do with the motion of a particle whose orbit brings it close to $r = 0$. As shown by the dashed line in Fig. 1, a particle whose position is measured in r shows very rapid
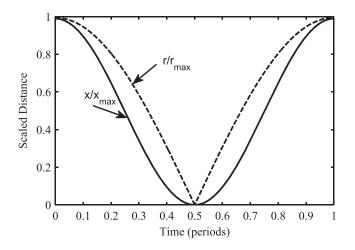

FIG. 1. The motion of an object which comes close to the origin displayed both in r and in $x = r^2$. The dashed line shows the motion in r, the solid line in x. A simulation must use very small time steps to resolve the motion at small r, whereas it can use larger time steps to resolve the motion if it is measured in x.

changes in r when it passes near the origin. Resolving such motion requires very short time steps. If the independent variable is $x = r^2$, however, motion like that shown by the solid line in Fig. 1 is obtained; it is smooth and does not require short time steps to resolve. Another benefit of using x instead of r is that there are roughly equal numbers of particles in each cell in x, whereas there are many fewer particles/cell at small r when r is the independent variable. This decreases the shot noise in the simulation near the origin.

Since the code uses the variable x, the particle mover in the code must be modified to work in this variable. The Lagrangian for this system in r and θ is

$$\mathcal{L} = \frac{m}{2}\left(\dot{r}^2 + r^2\dot{\theta}^2\right) + \frac{1}{2}m\omega_c r^2\dot{\theta} - q\phi, \quad (1)$$

where $\omega_c = qB/m$ and ϕ are the electrostatic potential. The canonical angular momentum is

$$P_\theta = mrv_\theta + \frac{1}{2}m\omega_c r^2, \quad (2)$$

where $v_\theta = r\dot{\theta}$. P_θ is a conserved quantity for each particle, because θ is an ignorable coordinate in the Lagrangian.

The variable r is eliminated by substituting $r = \sqrt{x}$ and $\dot{r} = \dot{x}/(2\sqrt{x})$ into the Lagrangian. After the equation of motion for x is calculated, Eq. (2) can be used to eliminate v_θ in favor of P_θ, giving

$$\ddot{x} = \frac{1}{2}\frac{\dot{x}^2}{x} - \frac{1}{2}x\omega_c^2 + \frac{2P_\theta^2}{m^2 x} + 2\frac{q}{m}\sqrt{x}E(x) = \frac{1}{2}\frac{\dot{x}^2}{x} + F(x). \quad (3)$$

$F(x)$ as defined by this equation depends only on x and not on $\dot{x}$. The leapfrog algorithm is used to advance the position and velocity, using $\dot{x} = v$ and $\dot{v} = \frac{1}{2}v^2/x + F(x)$. Because of the v^2 on the right-hand-side of the velocity equation, it must be finite-differenced implicitly. The x advance can be explicit. The time-advance equations are

$$v_{n+1/2} = -v_{n-1/2} + \frac{4x_n}{\tau}$$
$$- \frac{2}{\tau}\sqrt{4x_n^2 - 4x_n v_{n-1/2}\tau - 2F(x_n)x_n\tau^2} \quad (4)$$

and

$$x_{n+1} = x_n + \tau v_{n+1/2}, \quad (5)$$

where the subscripts on x and v indicate the time levels of each quantity and where τ is the size of the time step. Using Eq. (2), v_θ for each particle at time step $n + 1$ can be calculated by using the conserved P_θ for that particle

$$v_{\theta_{n+1}} = \frac{P_\theta}{m\sqrt{x_{n+1}}} - \frac{1}{2}\sqrt{x_{n+1}}\omega_c. \quad (6)$$

The operation of the code proceeds as follows. The code is initialized with approximately 1×10^6 particles, weighted appropriately for the desired density. Each particle is given a position in x consistent with the equilibrium density distribution. Each is also given a thermal v_r and v_θ, as well as an

additional v_θ from the equilibrium plasma rotation. The v_θ for each particle is converted into the appropriate P_θ, which is stored and which is conserved in the motion of that particle. Each particle is then given a perturbed $v_{1r}(x)$ as the initial condition of the mode being launched. The total v_r is converted to v_x and stored. At each time step, the density of the plasma is calculated by casting the particles onto a grid in x. The electric field is calculated by using Gauss' law on the enclosed charge at each x on the grid. The particles are then moved one time step by the mover as outlined above using interpolated values of $E(x)$ from the grid, and the process is repeated. Periodically the code calculates the radial electric field, $E(r)$, the radial and θ fluid velocities, $v_r(r)$ and $v_\theta(r)$, the fluid density, $n(r)$, and the three independent values of the pressure tensor, $P_{rr}(r)$, $P_{\theta\theta}(r)$ and $P_{r\theta}(r)$, and writes them out into a file for later analysis. Results from the simulation will be discussed in Sec. IV.

III. KINETIC THEORY OF THE MODES

A. Equilibrium

The non-neutral plasma equilibrium considered is the standard global thermal equilibrium in an infinitely long geometry[14] with distribution function (in two dimensions, v_r and v_θ, with $v^2 = v_r^2 + v_\theta^2$)

$$f_0 = \frac{n_0}{(2\pi)v_{th}^2}\exp\left[-\frac{v^2}{2v_{th}^2} - \frac{q(\phi(r) - \phi(0))}{k_BT} + \frac{\omega_0 P_\theta}{k_BT}\right], \quad (7)$$

where the plasma consists of particles with charge q, mass m, speed v, and temperature T, where n_0 is the central plasma density, k_B is Boltzmann's constant, and where $v_{th} = \sqrt{k_BT/m}$. The frequency ω_0 is the rigid rotation frequency. The plasma is confined by an axial magnetic field B so that the cyclotron frequency is given by $\omega_c = qB/m$. The canonical angular momentum is given by Eq. (2), which allows the distribution function to be written in the form

$$f_0 = \frac{n_0}{(2\pi)v_{th}^2}\exp\left[-\frac{v_r^2 + (v_\theta - \omega_0 r)^2}{2v_{th}^2}\right.$$
$$\left. + \frac{r^2}{2v_{th}^2}(\omega_0^2 + \omega_0\omega_c) - \frac{q(\phi(r) - \phi(0))}{k_BT}\right]. \quad (8)$$

Integrating this distribution function over all velocities to obtain the density, $n(r)$, and solving the resulting Poisson equation for $\phi(r)$ admit solutions with nearly constant density inside a region of plasma radius r_p bounded by a narrow transition (if the Debye length is small compared to the plasma radius) with a width of a few Debye lengths over which the density drops to zero. Such an equilibrium is only possible if the second and third terms in the exponential in Eq. (8) add very nearly to zero inside the plasma. Solving Poisson's equation for a constant interior density n_0 results in an electrostatic potential proportional to r^2. This gives the following condition on the rotation frequency ω_0, which ensures that these two terms add to zero inside the plasma:

$$\omega_0^2 + \omega_0\omega_c + \frac{1}{2}\omega_p^2 = 0, \quad (9)$$

where the plasma frequency ω_p is defined to be its value at the center of the plasma, $\omega_p = \sqrt{n_0q^2/\epsilon_0 m}$ and where ϵ_0 is the permittivity of free space. This condition on the rigid rotor frequency ω_0 results in 2 solutions. The lower frequency root is of interest in the work presented here and is given by

$$\omega_0 = -\frac{\omega_c}{2} + \frac{1}{2}\sqrt{\omega_c^2 - 2\omega_p^2} = -\frac{\omega_c}{2}(1 - \sqrt{1 - \beta}), \quad (10)$$

where $\beta = 2\omega_p^2/\omega_c^2$ is a measure of how close the equilibrium is to the Brillouin limit at $\beta = 1$. The narrow transition region at the edge of the plasma is produced when the plasma runs out of particles and the electrostatic potential ϕ drops below its central r^2-behavior, causing the exponential in Eq. (8) to quickly drop to zero. (Note from Eq. (9) that the second term in the argument of the exponential function is negative; the third is positive.)

B. $m = 0$ modes including finite Larmor radius

A kinetic theory will now be developed for the frequencies of $m = 0$ modes ($e^{i(m\theta - \omega t)}$) including the effects of finite Larmor radius $r_L = v_{th}/\omega_c$. The theory starts with the linearized Vlasov equation

$$\frac{Df_1}{Dt} = -\frac{q}{m}E_{1r}\frac{\partial f_0}{\partial v_r}, \quad (11)$$

where the advective derivative on the left is taken along the unperturbed orbits in phase space. In the interior of the plasma where the density is uniform, the equilibrium electric field is given by

$$E_0(r) = \frac{qn_0r}{2\epsilon_0}. \quad (12)$$

The particle orbit that at time $t' = t$ is at radial location r with radial velocity $v_r = v\cos\phi$ and azimuthal velocity $v_\theta = v\sin\phi$ is given by

$$r^2(t' - t) = r^2 + \frac{2rv}{\omega_v}(\sin(\omega_v(t' - t) - \phi) + \sin\phi)$$
$$+ \frac{4v^2}{\omega_v^2}\sin^2(\omega_v(t' - t)/2), \quad (13)$$

where

$$\omega_v = \sqrt{\omega_c^2 - 2\omega_p^2} = \omega_c\sqrt{1 - \beta}. \quad (14)$$

As discussed in Sec. II, and as can be seen in Eq. (13), $x = r^2$ is a convenient variable with smooth time dependence and no sharp spikes; it will be used throughout this calculation. The kinetic theory will need the radial velocity, which can conveniently be written as

$$v_r(\tau) = \frac{1}{2\sqrt{x(\tau)}}\frac{d}{dt}x(\tau)$$
$$= \frac{1}{2\sqrt{x(\tau)}}\left(2\sqrt{x(0)}v\cos(\omega_v\tau - \phi) + \frac{2v^2}{\omega_v}\sin\omega_v\tau\right), \quad (15)$$

where the quantity τ is given by $\tau = t' - t$. Integrating along the unperturbed orbits in τ from $-\infty$ to 0 (t' runs from $-\infty$ to t) and assuming that both f_1 and E_{1r} are proportional to $e^{-i\omega t'}$ yield

$$f_1 = \int_{-\infty}^{0} \frac{q}{m} \frac{E_{1r}(\tau) v_r(\tau)}{v_{th}^2} f_0 e^{-i\omega\tau} d\tau. \quad (16)$$

It is convenient to choose to describe the first-order radial electric field in terms of the quantity

$$G = E_{1r}(x)/\sqrt{x}, \quad (17)$$

which yields for f_1 the formula

$$f_1 = \int_{-\infty}^{0} \frac{q}{m} \frac{G(x(\tau))}{2v_{th}^2} \frac{dx(\tau)}{d\tau} f_0 e^{-i\omega\tau} d\tau, \quad (18)$$

taken along the unperturbed particle orbit of Eq. (13).

To perform this integral, $G(x(\tau))$ can be expanded in powers of the Larmor radius by writing

$$x(\tau) = x + \delta x(\tau) \quad \text{and}$$

$$G(\tau) = G(x) + G'(x)\delta x(\tau) + \frac{1}{2}G''(x)(\delta x(\tau))^2 + \cdots, \quad (19)$$

where $\delta x(\tau)$ consists of the second and third terms on the right-hand side of Eq. (13) and where the symbol $'$ denotes differentiation with respect to x. (Note that this expression breaks down as β approaches 1 because the plasma becomes unmagnetized and the particle orbits become too large for this expansion to be valid.) Using this form, it is now possible to analytically perform the time integration in Eq. (18) term by term (remembering that f_0 is a function of the equilibrium constants of the motion and so comes out of the integral). The perturbed radial electric field E_{1r} is connected to the perturbed distribution function f_1 through Gauss's law and the continuity equation

$$\nabla \cdot \mathbf{E} = \frac{q}{\epsilon_0} n_1 \quad \text{and}$$

$$-i\omega n_1 + \nabla \cdot (n_0 \mathbf{v}) = 0 \quad \Rightarrow \quad E_{1r} = \frac{-iq}{\epsilon_0\omega} \int v_r f_1 d^3v \quad (20)$$

or

$$G = \frac{-iq}{\epsilon_0\omega r} \int v_r f_1 d^3v. \quad (21)$$

Putting all of this together and keeping terms through $O(r_L^2)$ yield a differential equation for $G(x)$ valid inside the plasma where the unperturbed orbits do not sample the plasma edge

$$axG'' + 2aG' + cG = 0, \quad (22)$$

where

$$a = \frac{12r_L^2\omega_p^2\omega_c^2}{(\omega^2 - \omega_v^2)(\omega^2 - 4\omega_v^2)} \quad \text{and} \quad c = 1 - \frac{\omega_p^2}{(\omega^2 - \omega_v^2)}. \quad (23)$$

After discarding a solution which is singular at $x = 0$ this equation has solution

$$G(x) \propto \frac{J_1(k\sqrt{x})}{k\sqrt{x}} \quad \text{with}$$

$$k = 2\sqrt{\frac{c}{a}} = \sqrt{\frac{(\omega^2 - \omega_c^2 + \omega_p^2)(\omega^2 - 4\omega_v^2)}{3\omega_c^2\omega_p^2 r_L^2}}. \quad (24)$$

Note that since r_L is so much smaller than r_p, the plasma radius, this dispersion relation predicts that any modes with values of kr_p of order 1 must have frequencies either near $\omega = \omega_{uh} = \sqrt{\omega_c^2 - \omega_p^2}$ or near $\omega = 2\omega_v$.

Since this dispersion relation comes from just the first 3 terms in a Taylor-series in r_L^2, it is important to know the sizes of the terms being neglected. The extended form of this differential equation, through fourth order in Larmor radius, can be written

$$\alpha/(k^2)\left(\frac{x^2 G''''}{6} + xG'''\right) + xG'' + 2G' + \frac{k^2}{4}G = 0, \quad (25)$$

where

$$\alpha = \frac{120\omega_c^2 k^2 r_L^2}{(9\omega_v^2 - \omega^2)}. \quad (26)$$

The theory presented in this paper is only valid when the leading term in Eq. (25) is small compared to the other three. Using $G(x) \propto J_1(k\sqrt{x})/k\sqrt{x}$ to test the size of the leading term for kr_p up to about 10 shows that

$$\frac{\alpha\left(\frac{x^2 G''''}{6} + xG'''\right)}{xG'' k^2} \lesssim 50k^2 r_L^2, \quad (27)$$

which is less than 1% for the cases studied in this paper. Even when this ratio is small, however, the higher-order derivatives in this equation introduce new solutions and change the singularities at the origin. A Frobenius analysis shows that of the four independent solutions to this linear differential equation two are singular at $x = 0$, one is regular but oscillates wildly in x as α approaches zero, and one connects smoothly to the Bessel-function solution as α approaches zero. It is straightforward to find the power-series solution to Eq. (25) corresponding to this physical fourth solution. It is

$$G(x) = \sum_{n=0}^{\infty} a_n(k^2 x)^n \quad \text{with} \quad a_0 = \frac{1}{2}, \quad a_1 = -\frac{1}{16} \quad (28)$$

and

$$a_{n+1} = \frac{a_n}{4(n+1)(n+2)} - \alpha \frac{n(n+5)}{6} a_{n+2}. \quad (29)$$

The apparent awkwardness of having a_{n+1} depends on a_{n+2} is solved by iterating. With $\alpha = 0$ this recursion relation generates the power series for $J_1(k\sqrt{x})/(k\sqrt{x})$. Using it again with a non-zero value of α and with a_{n+2} in the formula

coming from the Bessel-function series gives a new series a_n. This process may be repeated until convergence is obtained for $\alpha \leq 4$. For the cases studied in this paper, however, this analysis hardly matters because the difference between the simple Bessel-function solution of Eq. (24) and that of Eq. (28) is less than 0.1%.

Proceeding with the simple Bessel-function theory, the dispersion relation in Eq. (24) can be solved to find $\omega^2(k)$

$$\omega^2 = \frac{1}{2}\left(5\omega_c^2 - 9\omega_p^2 \pm \sqrt{(3\omega_c^2 - 7\omega_p^2)^2 + 12\omega_c^2\omega_p^2 k^2 r_L^2}\right),$$
(30)

valid as long as β is not close to one. In the limit where $r_L \ll r_p$ and assuming that the modes have variations on the order of the plasma radius r_p so that $kr_p \approx O(1)$ then $kr_L \ll 1$ and we may expand this expression to find for the two modes

$$\omega^2 = \frac{5}{2}\omega_c^2 - \frac{9}{2}\omega_p^2 \pm \left|\frac{3}{2}\omega_c^2 - \frac{7}{2}\omega_p^2\right| \pm \frac{3\omega_c^2\omega_p^2 k^2 r_L^2}{|3\omega_c^2 - 7\omega_p^2|}. \quad (31)$$

For k real the upper sign gives modes near, but slightly above, $2\omega_v$ for $\beta < 6/7$, and modes near, but slightly above, ω_{uh} when $\beta > 6/7$. For k real the lower sign gives modes near, but slightly below, the upper hybrid frequency ω_{uh} for $3\omega_c^2 > 7\omega_p^2$, or $\beta < 6/7$, and modes near, but slightly below, $2\omega_v$ when $\beta > 6/7$. This expansion breaks down when the two cold mode frequencies are equal at $3\omega_c^2 = 7\omega_p^2$, i.e., when $\beta = 6/7$. In this case, we have

$$\omega^2 = \frac{4}{7}\omega_c^2 \pm \frac{3}{\sqrt{7}}\omega_c^2 k r_L \quad (32)$$

so that the deviation away from the cold mode frequency is much larger near this mode crossing ($O(kr_L)$ instead of $O(k^2 r_L^2)$). If k is imaginary, as it turns out to be in one case discussed later, the thermal frequency shift caused by finite Larmor radius is reversed.

It should be noted that the dispersion relation in Eq. (24), when specialized to the case of small β and uniform plasma density, agrees with Eq. (106) in Dubin's recent paper,[9] both relations giving

$$\omega \approx \omega_c - \frac{\omega_p^2}{2\omega_c}(1 + k^2 r_L^2). \quad (33)$$

It is interesting to note that the dispersion relation for $k(\omega)$ in Eq. (24) can be obtained from Davidson's equation (4.225) (Ref. 2) by setting his azimuthal mode number ℓ to zero and by keeping terms in his equation through $O(k_\perp^2 r_p^2)$, which only requires that terms from $n = -2$ to $n = 2$ be kept in the sum. This is somewhat surprising since Davidson's eigenfunctions are of form $e^{i\mathbf{k}\cdot\mathbf{r}}$ and his theory is restricted to the case $k_\perp r_p \gg 1$ while the mode differential equation (22) is cylindrical, leads to Bessel functions, and allows $k_\perp r_p \simeq 1$. This equivalence of Cartesian $k_\perp$ for sines and cosines with the radial mode number k for Bessel functions also occurs with the eigenvalue problem $\nabla^2\phi = \lambda\phi$, however, and the same thing apparently happens in the problem

at hand. If the kinetic theory described here is extended through $O(k^4 r_L^4)$, however, the mode dispersion relation in Eq. (22) contains the new term in Eq. (25) which is singular at $\omega = 3\omega_v$, just as a is singular at $\omega = 2\omega_v$. Bessel's equation is, then, no longer obtained and Davidson's dispersion relation does not describe the long wavelength modes. These higher order resonances at $3\omega_v$ and up are not studied in detail in this paper.

C. Fluid moments

With $G = E_{1r}/r$ in hand, it is straightforward to use Eq. (18) to solve for the perturbed distribution function f_1 and then to find the physically important fluid moments consisting of the perturbed velocities v_{1r} and $v_{1\theta}$, the perturbed density n_1, and the perturbed pressure tensor elements P_{1rr}, $P_{1\theta\theta}$, and $P_{1r\theta}$. In making this calculation, care must be taken to make sure that all terms through $O(r_L^2)$ are kept. The fluid moments through this order are found to be (using the dispersion relation, Eq. (24))

$$v_{1r} = \delta v J_1(kr), \quad v_{1\theta} = -i\delta v \frac{\omega_v(4\omega^2 - \omega_c^2 - 3\omega_v^2)}{2\omega(\omega^2 - \omega_v^2)} J_1(kr),$$
(34)

$$n_1 = -i\delta v \frac{kn_0}{\omega} J_0(kr), \quad E_{1r} = -i\delta v \frac{qn_0}{\omega\epsilon_0} J_1(kr), \quad (35)$$

$$P_{1rr} = -i\delta v \frac{k\omega_p^2 n_0 k_B T}{\omega(\omega^2 - \omega_v^2)(\omega^2 - 4\omega_v^2)}$$
$$\times \left[(3\omega^2 - 6\omega_v^2)J_0(kr) - (2\omega^2 + 4\omega_v^2)\frac{J_1(kr)}{kr}\right],$$
(36)

$$P_{1\theta\theta} = -i\delta v \frac{k\omega_p^2 n_0 k_B T}{\omega(\omega^2 - \omega_v^2)(\omega^2 - 4\omega_v^2)}$$
$$\times \left[(\omega^2 - 10\omega_v^2)J_0(kr) + (2\omega^2 + 4\omega_v^2)\frac{J_1(kr)}{kr}\right],$$
(37)

and

$$P_{1r\theta} = -3\delta v \frac{k\omega_p^2 \omega_v n_0 k_B T}{(\omega^2 - \omega_v^2)(\omega^2 - 4\omega_v^2)}\left[J_0(kr) - 2\frac{J_1(kr)}{kr}\right].$$
(38)

It is straightforward to show that these moments satisfy the perturbed continuity and momentum equations inside the plasma where n_0 and P_0 are constant

$$\frac{\partial n_1}{\partial t} + \nabla \cdot (n_0 \mathbf{v}_1) = 0 \quad \text{and}$$

$$m\left[\frac{\partial \mathbf{v}_1}{\partial t} + (\mathbf{v} \cdot \nabla \mathbf{v})_1\right] = q\mathbf{E}_1 + q\mathbf{v}_1 \times \mathbf{B} - \frac{1}{n_0}\nabla \cdot \mathbf{P}_1,$$
(39)

where $\mathbf{P}_1$ is the anisotropic perturbed pressure tensor.

Note that these terms in the pressure tensor are very different from the ones that would be obtained from the ideal fluid equation with an isotropic scalar pressure

$$P_1 = -i\gamma P_0 (\nabla \cdot \mathbf{v}_1)/\omega. \qquad (40)$$

The cyclotron orbits make the pressure tensor anisotropic and change the first-order dynamics completely. The simulations show, however, that near the upper-hybrid mode frequency, $\omega^2 \approx \omega_c^2 - \omega_p^2$, for the case of $\beta = 6/7$, there is a mode with $kr_p \approx 0$. This is a simple "breathing" mode and the pressure tensor elements for this mode in the $kr_p = 0$ limit satisfy $P_{1r\theta} \approx 0$, $P_{1rr} \approx P_{1\theta\theta}$, and $P_{1rr} \approx -i\gamma P_0 (\nabla \cdot \mathbf{v}_1)/\omega$ with $\gamma = 2$. This means that this simple breathing mode ($v_{1r} \propto r$) at the upper-hybrid frequency has an adiabatic pressure response appropriate for 2 degrees of freedom. This simple breathing mode is only found at $\beta = 6/7$, however.

D. The boundary condition at the plasma edge

The simulations produce modes with a discrete spectrum, as expected for a finite system. To find these mode frequencies, it is necessary to impose a boundary condition at the edge of the plasma. The particle orbits near the boundary are very different from those in the interior and the perturbed electric field, density, and pressure tensor may change rapidly as the plasma edge is approached. This makes the kinetic theory difficult to do there. It is possible, however, to obtain approximate equations that determine the values of kr_p for the observed modes by making a simple assumption about the way the perturbed pressure tensor behaves in the edge.

The calculation begins with the fluid momentum equations. The linearized radial and angular momentum equations in the Eulerian picture, including terms due to the radial variation of $n_0(r)$ and $P_0(r)$ in the plasma edge, can be written

$$m(-i\omega v_{1r} - 2\omega_0 v_{1\theta}) = qv_{1\theta}B + qE_{1r} - \left(\frac{\nabla \cdot \mathbf{P}_1}{n_0(r)}\right)_r$$
$$+ \frac{n_1}{n_0^2(r)}\frac{\partial P_0(r)}{\partial r} \qquad (41)$$

and

$$m(-i\omega v_{1\theta} + 2\omega_0 v_{1r}) = -qv_{1r}B - \left(\frac{\nabla \cdot \mathbf{P}_1}{n_0(r)}\right)_\theta. \qquad (42)$$

To handle these equations in the plasma edge we need expressions for both $n_0(r)$ and $P_0(r)$. The latter can be obtained if $n_0(r)$ is known through the ideal gas law $P_0(r) = n_0(r)k_BT$. The required expression for $n_0(r)$ comes from the plasma equilibrium equation

$$\nabla^2 \phi = -\frac{q}{\epsilon_0} n_0(r)$$
$$= -\frac{qn_0}{\epsilon_0}\exp\left[\frac{mr^2}{2k_BT}(\omega_0^2 + \omega_0\omega_c) - \frac{q(\phi(r) - \phi(0))}{k_BT}\right]. \qquad (43)$$

The equilibrium density $n_0(r)$ is nearly constant inside the plasma then falls off rapidly in r on the scale length of the Debye length near $r = r_p$. It is convenient to define a scaled

radial variable ξ in the edge by $r = r_p + \lambda_D\xi$ and to define the new dependent variable

$$g = \frac{q(\phi(r) - \phi(0))}{k_BT} - \frac{mr^2}{2k_BT}(\omega_0^2 + \omega_0\omega_c). \qquad (44)$$

Because $\lambda_D \ll r_p$ the Laplacian in the edge may be approximated by $\nabla^2 \approx (1/\lambda_D^2)\partial^2/\partial\xi^2$ to obtain the following approximate equilibrium equation for $g(\xi)$:

$$g'' = 1 - e^{-g} \quad \text{and} \quad n(\xi) = n_0 e^{-g} \quad \text{with}$$
$$g(0) = \ln 2 \quad \text{so that } n|_{\xi=0} = n_0/2. \qquad (45)$$

The function $g(\xi)$ is very nearly zero inside the plasma where $\xi \ll -1$ and $g(\xi) \propto \xi^2/2$ for large positive ξ beyond the plasma edge. The important quantity $g'(\xi)$ is also zero inside the plasma and makes the transition to $g' \approx \xi$ over a few Debye lengths through the plasma edge.

It is convenient to solve Eq. (42) for $v_{1\theta}$ to eliminate this variable from Eq. (41). The variables E_{1r} and n_1 may then be eliminated in favor of v_{1r} by using the exact expressions

$$E_{1r} = \frac{-iq}{\epsilon_0\omega} n_0(r)v_{1r} \quad \text{and} \quad n_1 = \frac{-i}{\omega r}\frac{\partial}{\partial r}(rn_0(r)v_{1r}). \qquad (46)$$

The terms involving the perturbed pressure tensor elements are more difficult because they depend critically on the details of particle orbits, but an analysis of the simulation results shows that the Lagrangian perturbed pressure tensor elements (these elements in the moving frame of the plasma edge) are given to a reasonable approximation by the fluid expressions in Eqs. (36)–(38), with the replacements

$$\delta v J_1(kr) = v_{1r}, \quad k\delta v J_0(kr) = \frac{1}{r}\frac{\partial}{\partial r}(rv_{1r}), \quad \text{and}$$
$$n_0 = n_0(r). \qquad (47)$$

Note that this assumes that the connection between $\mathbf{P}_1$ and v_{1r} in the edge is the same as it is in the interior, even though the particle orbits in the edge are much different than those in the interior. Precision in the determination of kr_p for the modes cannot be expected under this assumption.

Converting these Lagrangian expressions to their Eulerian counterparts through

$$P_{1rr}^E = P_{1rr}^L - \left(\frac{iv_{1r}}{\omega}\right)\frac{\partial P_0(r)}{\partial r},$$
$$P_{1\theta\theta}^E = P_{1\theta\theta}^L - \left(\frac{iv_{1r}}{\omega}\right)\frac{\partial P_0(r)}{\partial r}, \quad \text{and} \quad P_{1r\theta}^E = P_{1r\theta}^L, \qquad (48)$$

where the superscripts "E" and "L" denote quantities in the Eulerian and Lagrangian pictures, then leads to a complicated mode differential equation in v_{1r} alone. The mode equation simplifies considerably by using the substitution

$$r_L^2 = \frac{\omega_p^2}{\omega_c^2}\lambda_D^2, \qquad (49)$$

the dispersion relation in Eq. (30), and the expressions $\omega_p^2 = (\beta/2)\omega_c^2$ and $\omega_v^2 = (1 - \beta)\omega_c^2$. It is also helpful to use the equilibrium identity

$$e^{-2g} = e^{-g}\left(1 - \lambda_D^2 \frac{d^2g}{dr^2}\right) \qquad (50)$$

to eliminate the troublesome term e^{-2g} when it arises. The mode differential equation can then be written as

$$\frac{d^2v_{1r}}{dr^2} + \frac{1}{r}\frac{dv_{1r}}{dr} + \left(k^2 - \frac{1}{r^2}\right)v_{1r}$$
$$- \left(r\frac{dv_{1r}}{dr} - \frac{2[6(1-\beta) + \beta k^2\lambda_D^2]v_{1r}}{6 - 5\beta \pm \sqrt{(6-7\beta)^2 + 12\beta^2 k^2\lambda_D^2}}\right)\frac{1}{r}\frac{dg}{dr} = 0, \qquad (51)$$

where

$$\frac{dg}{dr} = \frac{1}{\lambda_D}\frac{dg}{d\xi}, \qquad (52)$$

and where the two choices for the sign in the denominator correspond to the modes near $2\omega_v$ and to those near ω_{uh}, as in the discussion following Eqs. (30) and (31).

Further simplification results by assuming that $k^2\lambda_D^2 \ll 1$ and expanding in this small quantity. In this approximation, the mode differential equation for the mode near $2\omega_v$ is found to be

$$\frac{d^2v_{1r}}{dr^2} + \frac{1}{r}\frac{dv_{1r}}{dr} + \left(k^2 - \frac{1}{r^2}\right)v_{1r} - \left[r\frac{dv_{1r}}{dr} - v_{1r}\right]\frac{1}{r}\frac{dg}{dr} = 0. \qquad (53)$$

For the mode near ω_{uh} in the same approximation, the result is

$$\frac{d^2v_{1r}}{dr^2} + \frac{1}{r}\frac{dv_{1r}}{dr} + \left(k^2 - \frac{1}{r^2}\right)v_{1r} - \frac{1}{\beta}\left[\beta r\frac{dv_{1r}}{dr} - 6(1-\beta)v_{1r}\right]\frac{1}{r}\frac{dg}{dr} = 0. \qquad (54)$$

Inside the plasma $dg/dr = 0$ and the solutions of these equations are simply $v_{1r} = \delta v J_1(kr)$ as we have seen before. Outside the plasma numerical experimentation shows that the solutions to these equations are generally rapidly growing and unphysical because they grow even faster than the equilibrium density $n_0(r)$ decreases. For particular values of k, however, the solutions are well-behaved and physical for $r > r_p$, which determines k and hence the mode frequencies. For $\lambda_D \ll r_p$ these special values of k are well-predicted by the condition that the multiplier of dg/dr in the mode differential equations vanishes when evaluated using the interior Bessel function solution $v_{1r} = \delta v J_1(kr)$ at $r = r_p$. The mathematical reason for this condition is that if the interior solution for some value of k does not result in the multiplier of dg/dr near the edge being small then the rapid increase in dg/dr moving through the edge kicks the solution rapidly toward either ∞ or $-\infty$.

The condition for the mode near $2\omega_v$ when $k\lambda_D \ll 1$ is

$$\omega \approx 2\omega_v : 2\frac{J_1(kr_p)}{kr_p} - J_0(kr_p) = J_2(kr_p) = 0. \qquad (55)$$

Note that the simplest root of this equation is $kr_p = 0$ which corresponds to $v_{1r} \propto r$. This would be a simple "breathing mode" at $\omega = 2\omega_v$, but the simulation never produces such a mode. Since the pressure tensor elements in the interior have a factor of $(\omega^2 - 4\omega_v^2)$ in their denominators, when ω approaches $2\omega_v$ they become singular unless the velocity-dependent terms in the numerator are very special. They are special in the interior, but there is no guarantee that they remain special in the edge. We conjecture that this breathing mode at $2\omega_v$ is an artifact of the assumption that the dependence of the pressure tensor on v_{1r} is the same in the edge as in the interior.

The mode condition for the upper-hybrid mode when $k\lambda_D \ll 1$ is

$$\omega \approx w_{uh} : (12 - 10\beta)\frac{J_1(kr_p)}{kr_p} - 2\beta J_0(kr_p)$$
$$= (6 - 7\beta)J_0(kr_p) + (6 - 5\beta)J_2(kr_p) = 0. \qquad (56)$$

It is interesting that the condition on the modes near $\omega = 2\omega_v$ does not depend on β. This is because for $k\lambda_D \ll 1$ the mode near $2\omega_v$ depends only on pressure restoring forces and not on the perturbed electric field. It should also be noted that the condition on the modes near ω_{uh} does depend on β and that for $\beta = 6/7$ this condition becomes identical to the condition for the modes near $2\omega_v$.

It is important to know how accurate these approximate conditions are compared to the more complete calculation involving solving the mode dispersion differential equation (51). Numerical experimentation shows that the errors introduced by not solving the mode differential equation and by not keeping terms of order $k^2\lambda_D^2$ when $r_p/\lambda_D > 40$ are all less than 1%, which turns out to be quite a bit less than the discrepancies between the values of kr_p predicted by Eqs. (55) and (56) and those obtained from the simulation (see Sec. IV). The calculation probably does not agree better with the simulation results because of the assumption that the pressure tensor elements have the same dependence on v_{1r} in the edge that they have in the interior.

The fundamental mode observed in the simulations is a special case of the upper-hybrid condition in Eq. (56). For $\beta > 6/7$ this condition predicts the fundamental value of kr_p, but for $\beta < 6/7$ the fundamental condition is obtained by letting k be imaginary, resulting in the condition

$$\omega \approx w_{uh} : (6 - 7\beta)I_0(|k|r_p) - (6 - 5\beta)I_2(|k|r_p) = 0$$
$$\text{for} \quad \beta < \frac{6}{7}. \qquad (57)$$

Note that when $\beta = 6/7$ the condition is $I_2(|k|r_p)$ which gives for the fundamental in this case $k = 0$, i.e., v_{1r} for this mode is simply proportional to r inside the plasma. This means that a simple "breathing" mode is only obtained at $\beta = 6/7$. It is interesting to consider the prediction of this condition for the fundamental as the plasma density becomes

small, i.e., as $\beta \to 0$. It predicts that $kr_p \to \infty$ which means that the fundamental is increasingly localized at the surface as β goes to zero. Expanding this condition in large $|kr_p|$ gives the approximate condition

$$|k|r_p \approx \frac{6}{\beta} - \frac{11}{2} - \frac{11}{256}\beta. \tag{58}$$

Because of the periodic nature of the Bessel functions J_0 and J_2 the zeroes of the roots of Eqs. (55) and (56) should be separated in kr_p by about π. Using this result in the approximate dispersion relation (31) then shows that the experimental signature of these modes at low β would be a cluster of frequencies near ω_{uh} and $2\omega_v$ separated roughly by

$$\delta\omega \approx B \frac{\omega_p^2}{\omega_c} \left(\frac{r_L}{r_p}\right)^2 (n+1), \tag{59}$$

where B is a number in the range of 5–10. The separation between modes increases linearly with the radial mode number $n = 1, 2, 3, \ldots$. Comparison between this theory and the simulation results will be given in Sec. IV B.

IV. SIMULATION RESULTS

A. Mode properties

Because the simulation was tied to a particular experiment, many of the parameters were tied to that experiment. The values used were $B = 0.43$ T, the mass and charge were that of a singly ionized Beryllium-7 ion, and the plasma radius was 2.0 cm. The temperatures used were 0.025 eV (room temperature), 0.2 eV, and 0.4 eV. All simulations were performed in SI units. The initial conditions of the simulation were for the plasma to be in equilibrium at a specified central density (which determines β) and temperature, with a small perturbed radial velocity added to the plasma. The perturbation was of the form $AJ_1(kr)$ where k was selected by experience to produce the desired mode. It is not necessary to choose the value of k very accurately; it is only necessary to be near the correct value for the desired mode to be launched. The simulation was then run for approximately 5000 cyclotron periods to get good frequency resolution of the modes. This is necessary because the modes are very closely spaced at colder temperatures and at values of β away from 6/7.

The data set to be analyzed consisted of radial profiles of v_{1r}, $v_{1\theta}$, n_1, P_{1rr}, $P_{1\theta\theta}$, $P_{1r\theta}$, and E_{1r} versus time. The analysis proceeded in two steps: first, accurate determination of the mode frequency and second, determination of the shape (in r) of the mode for each of the above quantities.

The frequency was determined by averaging each of the above quantities over a small region of space (such as from $r = 1.0$ cm to $r = 1.2$ cm) to reduce the shot noise produced by the finite number of particles and to produce a single curve of each quantity as a function of time. The curves were all then Fourier transformed with a FFT to produce an initial guess for the frequency. The data vs. time curves for all quantities were then simultaneously least-squares fit to their expected time dependence using a nonlinear least-squares algorithm. The

quantities v_r and $P_{1r\theta}$ were fit to $A\cos(\omega t + \phi)e^{-\gamma t}$ and the remaining quantities were fit to $A\sin(\omega t + \phi)e^{-\gamma t}$. Damping with decay rate γ was included because many of the modes are damped on the timescale of the simulation. The parameters of the fit were ω, γ, ϕ (which are common between all quantities) and the amplitudes of each of the quantities. This process gives between one and two more significant figures for the frequency than just taking the value given by the FFT. The amplitude and phase parameters are much more sensitive to noise in this process than is the frequency.

Once the frequency has been determined, the shape of the mode for each physical quantity can be calculated. This was done for each quantity by stepping through all the radial positions, using a nonlinear least-squares algorithm to fit the time history at that point to $A\sin(\omega t + \phi)$ or $A\cos(\omega t + \phi)$, depending on the quantity involved, where ω and ϕ were the values determined in the first step and where A was the only free parameter. Putting together the amplitudes at each radial position produces curves of mode shape vs. r for all seven of the quantities mentioned above.

The final step in the analysis of each mode was to fit all of the curves to their expected shapes as derived from the kinetic theory in Sec. III C, using the quantity k in the argument of $J_1(kr)$ and the amplitudes of the quantities as the free parameters.

Fig. 2 shows a typical FFT from one run of the simulation. This case was seeded with a velocity profile that is appropriate for a mode with one node in the plasma. There were two large modes that resulted, well separated in frequency. There were also some smaller contributions from modes with higher numbers of nodes as well. This pattern of having two modes with similar k is generally true for all of the modes, except for the one with no nodes in the plasma (which we call the fundamental mode). As shown near the end of Sec. III B, these modes must exist near either the Coriolis-shifted (by the equilibrium rotation and electric field) upper-hybrid frequency ($\omega_{uh} = \sqrt{\omega_c^2 - \omega_p^2}$) or near $2\omega_v = 2\sqrt{\omega_c^2 - 2\omega_p^2}$, twice the vortex frequency. The higher-frequency mode is above the higher of ω_{uh} and $2\omega_v$
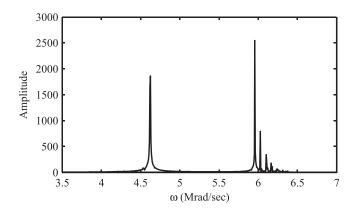

FIG. 2. FFT of v_r for a typical run of the simulation. This run was seeded for one node inside the plasma. Note the two large modes at different frequencies. This is typical of all runs that have nodes in the plasma. There are also some smaller contributions from modes with higher numbers of nodes in the plasma.
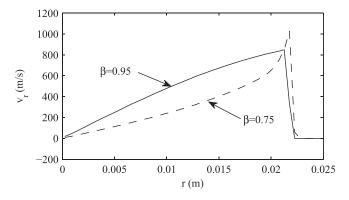
FIG. 3. The shape of v_{1r} for the fundamental mode at two values of β. The solid curve is for $\beta = 0.95$ and the dashed curve is for $\beta = 0.75$. The solid curve is well fit by $J_1(kr)$ out to $r = 0.02$ m and the dashed curve is well fit by $I_1(kr)$ out to $r = 0.018$ m. The curves drop to zero when the density of the plasma goes to zero.

and the lower-frequency mode is below the lower of these two frequencies. The one exception is the fundamental mode, which has a unique value of k at a given β and is always observed in the simulation to have a frequency just slightly above ω_{uh} (see the discussion near Eqs. (55) and (57)). Curves of ω_{uh} and $2\omega_v$ vs. β cross each other at $\beta = 6/7 \approx 0.857$. Both the simulation and the dispersion relation in Eq. (31), coupled with the boundary condition of Eq. (56), have the property that above $\beta = 6/7$ the fundamental behaves as $J_1(kr)$ and below it behaves as $I_1(kr)$, the modified Bessel function. This is because when ω is between ω_{uh} and $2\omega_v$ (when $\beta < 6/7$) then k, defined by Eqs. (23) and (24), becomes imaginary, which turns J_1 into I_1. This is shown in Fig. 3, where v_{1r} for the fundamental mode at $\beta = 0.95$ and $\beta = 0.75$ are shown. The modified Bessel function peaks near the surface of the plasma. As β decreases, the magnitude of k increases and the fundamental mode becomes more and more localized to the surface.

Figure 4 shows curves of the frequencies of several modes vs. β for $T = 0.025$ eV [part (a), where $r_p/r_L = 202$] and $T = 0.2$ eV [part (b), $r_p/r_L = 71$]. The upper-hybrid frequency is the green dashed line that runs to $1/\sqrt{2}$ at $\beta = 1$. The red dashed line is the line of $2\omega_v$. The + and $\times$ symbols

mark the frequencies of modes as seen in the simulation. The solid lines connect modes with the same number of radial nodes, n. The fundamental, marked by the symbol $\times$, is nearest to the upper-hybrid frequency and modes with $n = 1$, 2, and 3 are shown in the plot with the symbol +. Modes with increasing n are farther from both the upper-hybrid frequency and $2\omega_v$. Note that increasing temperature also moves the modes farther from each other, as expected. The lower modes are not shown for β near 1 because those modes are too heavily damped to be seen in the simulation. Modes for $\beta < 0.5$ are not plotted on these graphs because the modes are so closely spaced and close to their respective resonances that they cannot be seen as separate values on the plots. At $\beta = 0.1$ the modes are so closely spaced that they cannot be resolved in the simulation, even with a run of ~ 5000 oscillation cycles, but they may be able to be seen experimentally. Note that near $\beta = 6/7$ the spacing between the modes is much greater than it is in other regions of the plot. This is as predicted in Eq. (32) where the spacing is predicted to be of $O(kr_L)$ instead of $O(k^2 r_L^2)$ as is the case away from $\beta = 6/7$.

Figure 5 shows the shape of v_{1r} for the two $n = 1$ modes at $\beta = 0.75$ at a temperature of 0.2 eV. The labels "upper" and "lower" refer to high and low frequency, respectively. The solid lines are the data from the simulation; the dashed lines are the best Bessel function fits. The two modes have slightly different k's, but otherwise look similar. They differ in how they behave in the edge region, but describing these differences theoretically requires a detailed kinetic theory of the edge.

Figure 6 shows P_{1rr}, $P_{1\theta\theta}$, and $P_{1r\theta}$ for the higher frequency mode at $\beta = 0.75$. Note that the pressure is not at all isotropic. The solid curves show the theoretical pressure terms from Eqs. (36)–(38) and the dotted lines show the results of the simulation. Clearly the theory works well for this mode, until the edge of the plasma, beyond 0.018 m.

One obvious question to ask about these two modes is that if they have different frequencies but almost the same values of k, what is the physical difference between them? If they are launched with just a v_r perturbation at $t = 0$, both

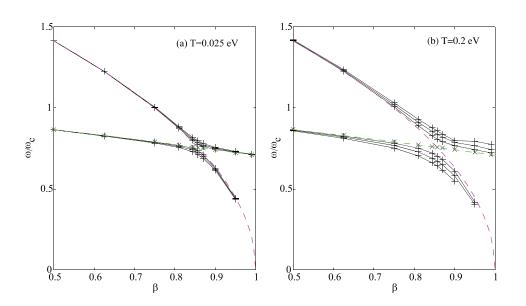FIG. 4. Frequencies of different modes as a function of β. The dashed curves are the upper-hybrid frequency (green) and $2\omega_v$ (red). The + symbols mark the frequencies seen in the simulation. The solid lines connect modes that have the same n's, where n is the number of radial nodes inside the plasma. The fundamental in both curves is shown by the $\times$ symbols near the upper hybrid frequency. The lower modes are not shown for β near 1 because those modes are too heavily damped to be seen in the simulation.
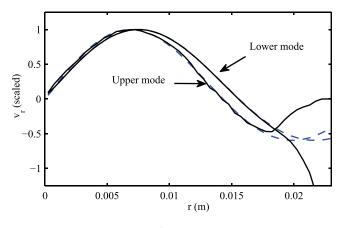
FIG. 5. v_{1r} for the $n = 1$ modes at $\beta = 0.75$ and $T = 0.2$ eV. The modes are shown with the solid lines. The dashed lines are the best fit to a $J_1(kr)$ Bessel function. Note that both have almost the same k, but behave differently in the boundary. The high frequency mode near $2\omega_v$ is the upper mode while the lower frequency mode at ω_{uh} is the lower mode.

modes are present in the final state. Almost all of the other fluid quantities are 90° out of phase with v_r, and so are not seeded at $t = 0$. The solution is found in the perturbed distribution function. The quantity $P_{1r\theta}$ from Eq. (38), the off-diagonal term in the pressure tensor, is in phase with the radial velocity v_r, and so needs to be included in the initial conditions to launch just one mode. The two modes in Fig. 5 have similar v_{1r} profiles, but almost opposite $P_{1r\theta}$ profiles. If a perturbation is launched with only a small radial velocity, a linear combination of these two modes will be produced, such that their profiles of $P_{1r\theta}$ add to zero. This determines the relative magnitude of the two modes in the simulation, as well as contributing to some of the higher n modes that appear in Fig. 2.

To test this hypothesis, a variant of the simulation was written that loads the particles differently. Rather than loading a 2D Maxwellian velocity distribution and adding $v_{1r}(r)$ to each particle, the code loaded the particles using the perturbed distribution function, $f_1(v_r, v_\theta)$, which is known from the kinetic theory. The f_1 that was used was simplified by only including the terms that contributed to the physical moments v_r and $P_{1r\theta}$.
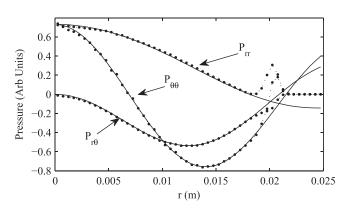
The integral of f_1 in ϕ, the gyro-angle in velocity space, is zero, which means that there are the same number of particles at each total velocity as before; they are just distributed differently in gyro-angle. The old distribution was uniform in ϕ, while the new distribution has an angular dependence. Figure 7 shows such a perturbed distribution function from the initial load of particles in this modified simulation for the higher mode shown in Fig. 2. For a perturbation where $P_{r\theta} = 0$, the peaks should be symmetric around $v_\theta = 0$. Note that the positive peak is not centered on $v_\theta = 0$, but rather is skewed to the right. The negative peak is similarly skewed to the left in v_θ. This is the effect of the non-zero $P_{r\theta}$ in this system.

Figure 8 shows the FFT of this single-mode simulation for two runs, one where it was launched to select out the higher frequency mode shown in Fig. 2 (the top graph) and the other when the lower mode frequency was selected (the bottom graph). Each mode is launched cleanly, with only a small presence of the other mode. The other higher k modes are also substantially suppressed. These two initialization techniques [just loading $v_r(r)$ and loading the perturbed distribution function] give the same results for ω and k for both modes to within one part in 10^4.

B. Comparison with kinetic theory

The results of the simulation can be compared with the kinetic theory and with the boundary condition given in Sec. III D. Figures 9 and 10 show the comparison between the values of kr_p predicted by the conditions in Eqs. (55) and (56) and those obtained by simulation for a plasma with $\beta = 0.75$ and $r_L/r_p = 1/71 = 0.0140$. This corresponds to a temperature of 0.2 eV and a plasma radius of 2 cm. We do not show a plot of the frequencies, since they agree between the simulation and the theory to within a fraction of a percent. Figure 9 shows kr_p for both the $2\omega_v$
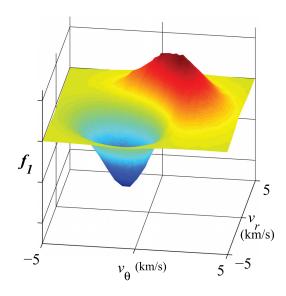

FIG. 6. P_{1rr}, $P_{1\theta\theta}$, and $P_{1r\theta}$ for the higher frequency mode of Fig. 5. The solid lines are the theoretical expressions and the dotted lines are the results from the simulation. Note that the pressure is clearly not isotropic and is not even diagonal.

FIG. 7. Surface plot of the perturbed distribution function of the higher-frequency mode shown in Fig. 5. This is used in initializing the particles for the single mode simulation. The v_θ-direction is right and left and the v_r-direction is in and out of the page. Note that the positive peak is shifted to the right from $v_\theta = 0$ and the negative peak is shifted to the left from $v_\theta = 0$. This is the effect of the nonzero $P_{1r\theta}$.
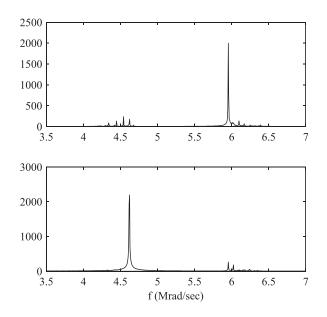
FIG. 8. FFT of data from the single mode simulation. Compare the FFT in Fig. 2. The top graph was for a run where the the higher mode was selected. The lower mode run is shown in the lower graph.

modes (black lines with circles) and the ω_{uh} modes (black lines with $+$ symbols). The theoretical values are shown in red. The dashed line is the prediction for the $2\omega_v$ modes and the dotted line is the prediction for the ω_{uh} modes. The modes are labeled by the number of nodes (n) within the plasma. Note that the long wavelength modes ($n = 1$) match much better than the higher n modes, and that the error increases as n increases. This is consistent with fact that the theory does not have the correct orbits in the edge region. Therefore as the wavelength approaches the size of the edge region, the theory does an increasingly poor job of matching the simulation.
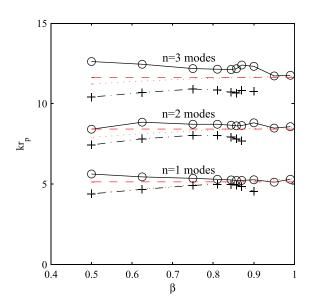
Figure 10 shows the comparison between theory and simulation for the fundamental mode. The theory is shown in the solid line and the dotted line with $+$ symbols is the simulation result. Below $\beta = 6/7$, the results are shown as negative values. This is the region where kr_p is a pure imaginary number. The values shown have the same magnitude as the imaginary kr_p. Above $\beta = 6/7$, the values of kr_p are real and correspond to the values plotted. We can see that the theory qualitatively captures the behavior of the mode, but is in error by about 20% for $\beta \geq 0.5$. It diverges rapidly from the simulation for $\beta < 0.5$. In this same region, the fundamental mode becomes damped with a damping time of roughly 1000 cycles. It appears that in this region some of the particles in the edge become resonant with the mode and therefore cause it to damp. The mode frequency is too low for $\beta > 0.5$ for a significant number of the particles to be in resonance with the mode. Below $\beta = 0.25$, it is not possible to resolve the modes from each other in the simulation because the damping of the modes and their decreasing spacing cause them to overlap significantly.

C. Higher temperature, higher resonances, and damping

As mentioned previously, the modes are spread farther apart at higher temperature, as shown in Fig. 11. This figure shows the frequency of the modes as determined by the simulation as a function of β for a temperature of $T = 0.4\,\text{eV}$ ($r_L/r_p = 1/50$). It also shows the interaction of higher order ($3\omega_v$, $4\omega_v$, etc.) resonances with these modes as the temperature increases. When the thermal effects pull the modes farther from ω_{uh} in the region for $\beta > 0.9$, it can be seen that the interaction with the higher order resonances becomes significant. When the thermal effects bring the frequency close enough to the resonance then that mode will be pulled to a
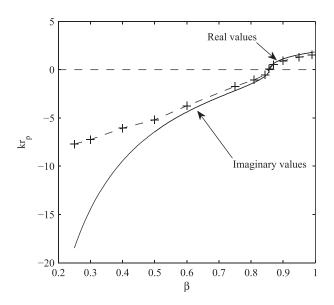

FIG. 9. kr_p vs. β at $T = 0.2\,\text{eV}$ for modes that have nodes in the plasma. The lines with circles are simulation results for the $2\omega_v$ modes. Lines with $+$ symbols are simulation results for the ω_{uh} modes. Red dashed lines are the theoretical results for $2\omega_v$ modes, and red dotted lines are the theoretical results for the ω_{uh} modes. The labels indicate the number of nodes in the plasma in each group of modes. The theory agrees much better at low n than it does at high n, where the wavelength approaches the width of the edge.

FIG. 10. kr_p vs. β for the fundamental mode at $T = 0.2\,\text{eV}$. Below $\beta = 6/7$ the values of kr_p are imaginary, here plotted as negative. The magnitude of kr_p is equal to the magnitude of the numbers plotted. Above $\beta = 6/7$ kr_p is real and is plotted accurately. Clearly the theory tends to overestimate the value of kr_p for the fundamental mode by about 20%.
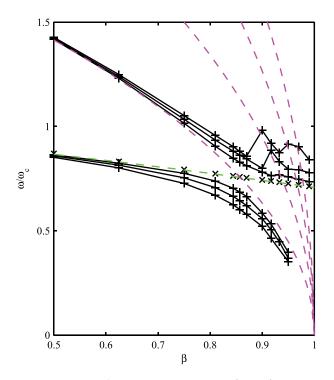
FIG. 11. Frequency vs. β for a $T = 0.4\,\text{eV}$ plasma ($r_L/r_p = 1/50$). Compare Fig. 4. The dashed curves are the upper-hybrid frequency (green) and multiples (2, 3, 4, 5) of ω_v (red). The $+$ symbols mark the frequencies seen in the simulation. The solid lines connect modes that have the same n's, where n is the number of radial nodes inside the plasma. The fundamental in both curves is shown by the $\times$ symbols near the upper hybrid frequency. Note the interaction of the modes with the higher order resonances at high β. The v_r for those modes where the interactions with the higher modes are important is still roughly of the form $J_1(kr)$, but the pressure terms do not fit the theory in this paper.

frequency above the resonance. This same effect can be seen less dramatically in Fig. 4 in the upper branch frequencies for $\beta = 0.95$ and 0.99.

The FFTs of v_{1r} also indicate resonances at higher multiples of ω_v. For example, the $n = 3$ mode at $\beta = 0.9$ is pulled above the $3\omega_v$ resonance, and there are indications in the FFT of this run of another mode near $4\omega_v$, although its shape and properties are hard to extract from the simulation data.[15] As would be expected from the fact that there are additional terms in the mode differential equation, the modes in this region no longer agree with the theory presented in Sec. III. These modes are not completely different, however. Many times v_{1r} still is approximately described by a $J_1(kr)$ Bessel function, but it has additional high-spatial-frequency wiggles in it. Even when v_{1r} and $v_{1\theta}$ still appear to be reasonably described by $J_1(kr)$, the pressure terms are very different in magnitude than the theory predicts in this region.

Many of these modes are damped, some heavily, with $2\pi\gamma/\omega$ of the order of 0.1. In general, the damping is higher at higher temperatures and the farther the mode's frequency is below the upper-hybrid frequency. The lower-branch modes are the most affected. The fundamental mode is weakly damped ($2\pi\gamma/\omega < 10^{-3}$) for $\beta < 0.5$. The energy from damped modes appears as random kinetic energy (the term temperature is poorly defined in this collisionless kinetic system) of the particles, mainly deposited in the regions of the plasma nearest the outer edge.

While not a part of the work reported here, it is interesting to note that a recent PIC simulation of these modes has been done in r-z geometry, so that the plasma has finite length.[12] Because of the finite length, and because electrostatic modes have potentials that vanish near the plasma ends,[11] k_z is non-zero and the electrostatic mode potential behaves as $\cos(k_z z)$, where $z = 0$ is the midplane of the plasma. This $\cos(k_z z)$ behavior extends to the electric field at the wall as well, so that the maximum induced surface charge density for a finite-z plasma occurs at the center of the plasma, rather than at the ends. This means that these modes in long plasmas could be detected near the center of the plasma and not only near the ends, as might be supposed by thinking about Gauss's law.

V. CONCLUSIONS

We have observed axisymmetric electrostatic Bernstein modes in a simulation of an infinite-length non-neutral cylindrical plasma. A kinetic theory has been developed that describes these modes well as long as the higher order resonances ($3\omega_v$, $4\omega_v$, etc.) are not important. There are three classes of modes: the fundamental, which is slightly higher than the upper-hybrid frequency $(\omega_c^2 - \omega_p^2)^{1/2}$, a high-frequency branch, and a low-frequency branch. The two branches are clustered near two frequencies: the upper-hybrid frequency and twice the Coriolis-shifted cyclotron frequency, $2\omega_v$. The low modes are below the lower of these two frequencies while the high modes are above the higher of these two frequencies. The frequencies cross each other at $\beta = 6/7$, and display classic mode-crossing behavior. At low β, the separation between adjacent modes is roughly given by $\delta\omega \approx B\omega_p^2/\omega_c (r_L/r_p)^2 (n+1)$, where B is a number in the range of 5–10 and n is the number of radial nodes in v_{1r}. The frequency of the lower modes decreases with higher k, while the frequency of the higher modes increases with higher k. The wavenumber k is only real when ω is less than both or greater than both ω_{uh} and $2\omega_v$. Between the two frequencies k is imaginary. This is true for the fundamental mode when $\beta < 6/7$, since the frequency of the fundamental is always observed in the simulation to be just slightly greater than ω_{uh}. The magnitude of k increases as β decreases in this region, making the fundamental more and more localized on the surface of the plasma, since $I_1(kr)$ increases exponentially with r. At typical experimental parameters, where β is usually $<10\%$, the fundamental would be difficult to see at all, as the oscillations would be almost entirely localized at the surface. Where k is real, as in the high and low branches of the modes and for the fundamental for $\beta > 6/7$, v_{1r} goes as $J_1(kr)$ and the pressure is highly anisotropic.

The simulation also shows several effects that are not included in this theory, including interactions with higher resonances of ω_v and damping of the modes.

[1]I. B. Bernstein, Phys. Rev. **109**, 10 (1958).

[2]R. C. Davidson, *Physics of Nonneutral Plasmas* (Addison Wesley, Redwood City, 1990), p. 159.

[3]S. A. Prasad, G. J. Morales, and B. D. Fried, Phys. Fluids **30**, 3093 (1987).

[4]A. J. Peurrung, R. T. Kouzes, and S. E. Barlow, Int. J. Mass Spectrom. Ion Process. **157**/**158**, 39 (1996).

[5]J. J. Bollinger, D. J. Heinzen, F. L. Moore, W. M. Itano, D. J. Wineland, and D. H. E. Dubin, Phys. Rev. A **48**, 525 (1993).

[6]R. W. Gould and M. A. LaPointe, Phys. Rev. Lett. **67**, 3685 (1991); Phys. Fluids B **4**, 2038 (1992); R. W. Gould, Phys. Plasmas **2**, 1404 (1995); **2**, 2151 (1995).

[7]D. L. Book, Phys. Plasmas **2**, 1398 (1995).

[8]D. H. E. Dubin, Phys. Rev. Lett. **66**, 2076 (1991).

[9]D. H. E. Dubin, Phys. Plasmas **20**, 042120 (2013).

[10]S. E. Barlow, J. A. Luine, and G. H. Dunn, Int. J. Mass Spectrom. Ion Process. **74**, 97 (1986); S. H. Lee, K. P. Wanczek, and H. Hartmann, Adv. Mass Spectrom. B **8**, 1645 (1980); D. L. Rempel, E. B. Ledford, S. K. Huang, and M. L. Gross, Anal. Chem. **59**, 2527 (1987).

[11]S. A. Prasad and T. M. O'Neil, Phys. Fluids **26**, 665 (1983).

[12]M. A. Hutchison, M.S. thesis, Brigham Young University, 2012.

[13]M. Takeshi Nakata, G. W. Hart, and B. G. Peterson, J. Am. Soc. Mass Spectrom. **21**, 1712–1719 (2010).

[14]R. C. Davidson, *Physics of Nonneutral Plasmas* (Addison Wesley, Redwood City, 1990), pp. 90–96.

[15]This is consistent with the discussion of Bernstein modes by Davidson in Ref. 2 above.